ELSEVIER

Journal of Luminescence 63 (1995) 85–96

JOURNAL OF LUMINESCENCE

Excited state absorption mechanisms of red to UV and blue conversion luminescence in Tm^{3+} doped fluorophosphate glass

G. Özen*, A. Kermaoui[a], J.P. Denis, Xu Wu[b], F. Pelle, B. Blanzat

Laboratoire de Physico-Chimie des Matériaux, CNRS, UPR-211, 1 Place Aristide Briand, 92190 Meudon, France

Received 10 January 1994; revised 22 June 1994; accepted 23 June 1994

Abstract

Characteristics and ion–ion interaction processes important in the optical dynamics of UV and blue upconversion luminescence in Tm^{3+} doped fluorophosphate glass have been investigated by exciting Tm^{3+} ions into the $^3F_2$ level with a DCM dye laser tuned at 657 nm. Two emission bands centered at 363, 451 nm from the $^1D_2$ level and one emission band centered at 478 nm from the $^1G_4$ level were observed. The 451 nm emission was stronger than the 478 nm emission. The excitation power dependence of all the upconverted emissions were found to be quadratic, conforming the two photon nature of these transitions. The mechanism leading to these emissions was attributed to the excited state absorption (ESA) from the $^3F_4$ and $^3H_4$ levels for the emissions of the $^1D_2$ and $^1G_4$ levels, respectively. The loss mechanism due to ion–ion interaction in the $^3F_4$ level therefore was studied as function of temperature by measuring the spectral overlap between emission and absorption spectra of this level. From this data relevant microscopic interaction parameters that give a measure of Tm–Tm coupling have been calculated. Optical properties of the intermediate and the final levels involved in the upconversion processes were studied using the Judd–Ofelt theory. This theory was also used to determine radiative transition rates and the fluorescence quantum efficiencies of the excited levels, and the excited state absorption coefficient for the $^3F_4 \rightarrow {}^1D_2$ and $^3H_4 \rightarrow {}^1G_4$ transitions when the excitation was fixed at 657 nm. Lower excited state absorption coefficient of the former transition explains why the 478 nm emission intensity is weaker than 451 nm emission intensity in this glass. According to the rate equation model temperature dependence of the upconverted emission intensities from the $^1D_2$ level was controlled by the temperature dependence of the excited state absorption coefficient corresponding to the $^3F_4 \rightarrow {}^1D_2$ transition.

1. Introduction

In the past few years, upconversion pumped lasers have attracted much research interest because of their applications in color displays, optical recording, biomedical diagnostics and underwater optical communication, etc. Lasing operation in a number of materials doped with rare-earth ions has been reported [1]. Glasses are one of the attractive hosts because they can be used to fabricate optical fibers and fiber lasers; they are transparent in a wide optical region and also large amounts of rare-earth ions can be introduced into the glass matrix.

* Corresponding author. At: Department of Physics, Faculty of Science and Letters, Istanbul Technical University, Maslak, Istanbul, Turkey.

[a] Permanent address: Laboratoire Laser, CDTA 2bd, BP 1017 Alger Gare, Algeria.

[b] Permanent address: Changchun Institute of Physics, Academia Sinica, Changchun, China.

SSDI 0022-2313(94)00043-3

Two main mechanisms for the upconversion processes are excited state absorption (ESA) and energy transfer (APTE) [2–4]. ESA is a two-step excitation process which occurs in several rare-earth ions. This mechanism depends linearly on the density of the excited ions because both absorption steps take place within the same single ion [5]. To study the ESA mechanism it is necessary to use two excitation beams; one called as the pump raises the ions from the ground state to an excited level, and the second called as the probe leads them from one metastable excited state to another one. If an emission results from this double absorption, the excitation spectra corresponding to the transitions between excited states can be obtained by measuring the anti-Stokes emission as function of the probe beam wavelength. In the literature, a single laser beam was also used as both pump and a probe beam, which eliminates the problem of the spatial beam coincidence [6–9].

Optical and lasing properties of upconverted emissions in Tm^{3+} doped fluoride glasses [10] and fluorozirconate glass fibers [11] have been studied by several researchers under red laser light excitation. Recently, the upconversion mechanisms for the blue emission from the $^1G_4$ level of Tm^{3+} in fluoroaluminate glasses was explained by including the cross-relaxation processes which occur from the $^3F_4$ level [12]. The cross relaxation occurs when a Tm^{3+} ion in the $^3F_4$ level relaxes to the $^3H_4$ level by exciting a nearby Tm^{3+} ion in the ground state to the $^3H_4$ level due to the ion–ion interactions. This level ($^3H_4$) acts as the intermediate level for the upconverted emissions from the $^1G_4$ level.

Auzel [13] has shown that the fluorescence lifetime of the metastable levels of rare earth ions in fluorophosphate glass could become longer than those measured in fluoride glasses, which can be explained by considering the destruction of OH^- during the glass preparation. Spectroscopic studies reported for Tm^{3+} in flourophosphate glasses also indicate that this can be a promising host matrix for laser action in the 450 nm spectral region ($^1D_2 \rightarrow {}^3H_4$ transition) [14,15]. Adding PbF_2 into the host may even increase the upconversion efficiency [16]. To obtain a laser emission in different hosts information is needed about the excitation mechanisms, optimum pump wavelengths, cross-relaxation coefficients, fluorescence lifetimes, radiative and non-radiative transitions and branching ratios [17].

In this work, we present the results of a comprehensive study of the upconversion emissions in a Tm^{3+} doped fluorophosphate glass, containing 27 mol.% PbF_2 by ESA mechanism. Fundamental properties of the upconverted emissions were explained in terms of the optical properties of the metastable levels of Tm^{3+} using the Judd–Ofelt theory [18,19] which has been shown to give reasonable results in the glass matrices [20] and a simple rate equation model. The solutions for these equations were obtained for the continuous excitation condition and were used to determine the temperature dependence of the transfer rate between $^3F_4$–$^1D_2$ and $^3H_4$–$^1G_4$ excited levels. Loss mechanisms for the upconverted emissions from the $^1D_2$ level due to the ion–ion interaction in the $^3F_4$ level were explained through the theoretical models developed by Dexter [21] and Inokuti–Hirayama [22].

2. Experimental

The general composition of the glass investigated in this work was (APbF:RE): $2.67(AlPO_4) + 37.33(AlF_3) + 27(PbF_2) + (33 - x)(CaF_2) + x(TmF_3)$ where x is 0.05, 0.1, 0.2, 0.3, 0.6, 1.0 and 1.5, TmF_3 concentrations in mol.% studied in this work which correspond to 0.106, 0.202, 0.423, 0.635, 1.267, 2.101 and 3.133 Tm^{3+} concentrations in $10^{20}\,cm^{-3}$, respectively. Preparation techniques were described elsewhere [23]. The experiments performed include absorption, emission and excitation spectra and, response to pulsed excitation measurements in the visible and infrared spectral region.

Optical absorption spectra were recorded using a Cary-17 spectrometer in the range of 320–2000 nm at room temperature. For the emission and excitation measurements either DCM dye laser (Coherent 5920) pumped with an Ar^+ laser (Coherent Innova 300) or a 150 W XBO Xe-lamp filtered by a Jobin–Yvon HD10 double monochromotor were used to excite the desired levels of Tm ions, respectively.

Emission from the sample was focused on the entrance slit of a Jobin–Yvon HR 1000 spectrometer and detected with a R649 Hamamatsu photomultiplier tube. Excitation spectra were recorded in the range of 620–700 nm where the ground state absorption bands of $^3F_2$ and $^3F_3$ levels are located according to the absorption spectrum of Tm^{3+} ions. The intensity of the excitation light was measured with a Coherent 200 power meter at the sample position.

The luminescence decays were measured using a Molectron dye laser with 5 ns duration pumped with a Sopra Nitrogen laser (Model 2001) as the excitation source. The signal was detected with an RTC 56 TVP photomultiplier tube and then analyzed by a PAR 162 boxcar integrator or a Tektronix model 7912AD digitizer interfaced with a PC-AT microcomputer.

For the low temperature measurements the sample was mounted in a CTI cryostat and the temperature was controlled using a closed cycle helium refrigerator and an LTS 21 type Lake Shore temperature controller. The sample temperature was varied from 11 to 300 K.

3. Spectroscopic properties of Tm^{3+}

The optical properties of Tm^{3+} ions in our glass have been studied using the Judd–Ofelt (JO) theory [18,19]. Absorption spectra of all the glasses were obtained at room temperature in the 300–2000 nm spectral range. Fig. 1 shows the absorption spectrum of the compound doped with 1 mol.% TmF_3. The shape and the position of each band are similar in each compound except the relative intensity of absorbance. The absorbance varies linearly with Tm^{3+} concentration. The bands correspond to the transitions from the ground state, $^3H_6$, to the different excited states of Tm^{3+} ions. The observed transition energies and the assignments for the absorption bands are given in Table 1 together with the measured and calculated intensities of the ground state absorption bands. The oscillator strengths (f) of the absorption bands, the Judd–Ofelt parameters and the radiative transition rates for the dipole–dipole transitions were determined in the same way used in Ref. [23]. The JO parameters are found to be $\Omega_2 = 1.38$, $\Omega_4 = 0.75$ and $\Omega_6 = 0.92 \times 10^{-20}\,cm^2$. The RMS deviation of the f-calculated from the f-measured values was calculated from the residuals (see Table 1). It is found to be 3.5×10^{-7} which is comparable to the RMS deviation obtained for other glasses [25].

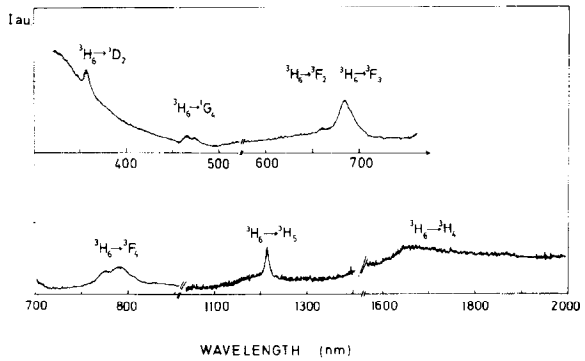

Fig. 1. Room temperature absorption spectrum of the glass doped with $2.101 \times 10^{20}\,cm^{-3}\,Tm^{3+}$ ions.

The total spontaneous emission probability, W_R, for an ith excited state is given as the sum of the $A(J, J')$ terms calculated over all terminal states which is related to the radiative lifetime τ_R and the branching ratio, β, of the level by $1/\tau_R(i) = \sum_j A(i, j) = W_R$ and $\beta = A(J, J')/W_R$, respectively. Table 2 presents the calculated emission probabilities, radiative lifetime and the branching ratios for the laser emission states ($^1D_2$ and $^1G_4$ levels) and the intermediate states involved in the upconversion processes ($^3F_4$ and $^3H_4$ levels) of Tm^{3+} ions in case of the electric dipole transitions. Branching ratio of the UV and the two blue emissions due to the $^1D_2 \rightarrow {}^3H_6$, $^1D_2 \rightarrow {}^3H_4$ and $^1G_4 \rightarrow {}^3H_6$ transitions are 36%, 49% and 38%, respectively. These values define the quantum efficiency of each transition which correspond to the laser transitions obtained in some Tm^{3+} activated materials [26].

The time development of the excited levels of Tm^{3+} ions was measured at room temperature by exciting the desired level directly as a function of the concentration. Fig. 2 presents the time

Table 1
Measured and calculated oscillator strengths of Tm^{3+} in fluorophosphate glass at room temperature. All transitions are from the $^3H_6$ level to the level indicated

Level	Wavelength [nm]	Average frequency [cm^{-1}]	Oscillator strength [10^{-8}]		Residual [10^{-8}]
			measured	calculated	
$^1D_2$	358	27933	116	105	−11
$^1G_4$	468	21391	86	34	−52
$^3F_2$	658	15196	198	213	15
$^3F_3$	683	14641	198	213	15
$^3F_4$	780	12820	164	142	−22
$^3H_5$	1189	8409	–	–	–
$^3H_4$	1695	5899	136	103	−33

The Judd–Ofelt parameters: $\Omega_2 = 1.38 \times 10^{-20}\,cm^2$; $\Omega_4 = 0.75 \times 10^{-20}\,cm^2$; $\Omega_6 = 0.92 \times 10^{-20}\,cm^2$. RMS $= 3.5 \times 10^{-7}$ and the refractive index = 1.56.

Table 2
Calculated spontaneous emission probabilities of Tm^{3+} in the fluorophosphate glass

Transition	Average frequency [cm^{-1}]	A_{ed}[s^{-1}]	t_R[ms]	β[ms]
$^1D_2 \rightarrow {}^3H_6$	27933	3360	0.107	0.360
$^3H_4$	22033	4590		0.491
$^3H_5$	19525	59		0.006
$^3F_4$	15113	636		0.068
$^3F_3$	13291	316		0.034
$^3F_2$	12736	319		0.034
$^1G_4$	6543	53		0.006
$^1G_4 \rightarrow {}^3H_6$	21390	330	1.14	0.376
$^3H_4$	15491	79		0.090
$^3H_5$	12982	340		0.390
$^3F_4$	8570	95		0.108
$^3F_3$	6949	28		0.032
$^3F_2$	6193	6		0.007
$^3F_4 \rightarrow {}^3H_6$	12821	510	1.78	0.562
$^3H_4$	6921	43		0.077
$^3H_5$	4412	9		0.016
$^3H_4 \rightarrow {}^3H_6$	5899	86	11.7	1.000

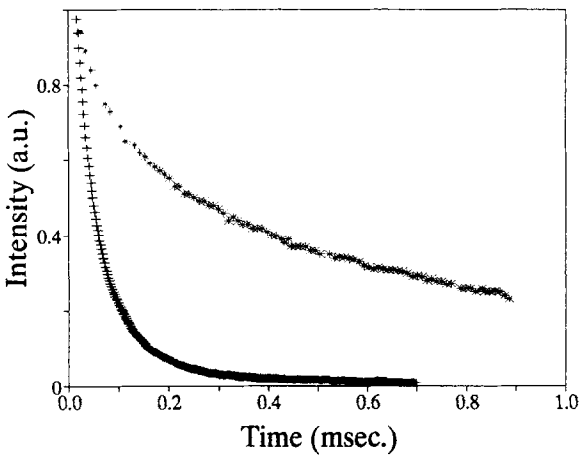

Fig. 2. Decay profiles of $^3F_4$ level in the compounds doped with (*): 0.423 and (+): $3.133 \times 10^{20}\,cm^{-3}\,Tm^{3+}$ ions which are equivalent to 0.2 and 1.5 mol.% TmF_3 concentrations, respectively ($T = 300$ K).

development of $^3F_4$ level for 0.2 and 1.5 mol.% TmF_3 concentrations at room temperature. The effect of the temperature on the decay profiles of the excited levels was also investigated in the sample doped with 0.2 mol.% TmF_3. All the curves were non-exponential for all the Tm^{3+} concentrations from 0.05 to 1.5mol.%. Therefore the average decay time of each level was determined by measuring the area under the curve after the initial value was normalized to unity to study the effect of Tm^{3+} concentration and temperature on the optical properties of the excited levels of Tm^{3+}. The values obtained are listed in Table 3. The Decay time of $^1D_2$ level is constant up to 1.0 mol.% and becomes shorter for higher concentrations. Decay times of

Table 3
Measured fluorescence lifetimes of the $^1D_2$, $^1G_4$, $^3F_4$ and $^3H_4$ levels of Tm^{3+} versus TmF_3 concentration (C_{Tm} denotes the Tm concentration)

C_{Tm}	Fluorescence Lifetime [ms]			
$[10^{20}\,cm^{-3}]$	$^1D_2$ level	$^1G_4$ level	$^3F_4$ level	$^3H_4$ level
0.106	0.044	0.450	1.000	1.800
0.202	0.043	0.467	0.908	1.900
0.423	0.044	0.417	0.693	1.500
0.635	0.041	0.411	0.756	1.400
1.267	0.043	0.414	0.514	1.100
2.101	0.042	0.402	0.418	1.000
3.133	0.039	0.383	0.355	0.890

the $^1G_4$ and $^3F_4$ levels are constant up to 0.3 and 0.6 mol.% TmF_3, respectively. Above these concentrations shorter decay times were observed.

4. Up- and down conversion luminescence upon 657 nm excitation

Fig. 3 shows the room temperature upconverted emission spectrum of the glass doped with 0.2 mol.% TmF_3 obtained when the $^3F_2$ level of Tm^{3+} was excited with 657 nm laser light. The bands observed are centered at 363, 451 nd 478 nm and they correspond to the $^1D_2 \rightarrow {}^3H_6$, $^1D_2 \rightarrow {}^3H_4$ and $^1G_4 \rightarrow {}^3H_6$ transitions, respectively. The strongest emission intensity was observed for the $^1D_2 \rightarrow {}^3H_4$ transition. In addition to the upconversion emission spectra the emission bands on the lower energy side of the excitation wavelength were also measured. Fig. 4(b) shows a doublet structured band centered 775 and 791 nm corresponding to the $^3F_4 \rightarrow {}^3H_6$ transition at room temperature. The spectra given in Fig. 4 were used to determine the critical interaction distance between Tm^{3+} ions for the $^3F_4$ level. The integrated intensity of this band varies linearly with excitation power (see Fig. 6).

The excitation spectra of the upconverted emissions from the $^1D_2$ level show a broad band centered at about 657 nm as seen in Figs. 5(a) and (b). Excitation spectra of upconverted blue emission from the $^1G_4$ level and down-converted emission from the $^3F_4$ level are also given in Figs. 5(c) and (d), respectively. The former spectrum shows two peaks centered at 647 and 657 nm. The excitation spectrum of the $^3F_4$ emission consists of two bands due to the $^3F_2$ and $^3F_3$ ground state absorptions as expected.

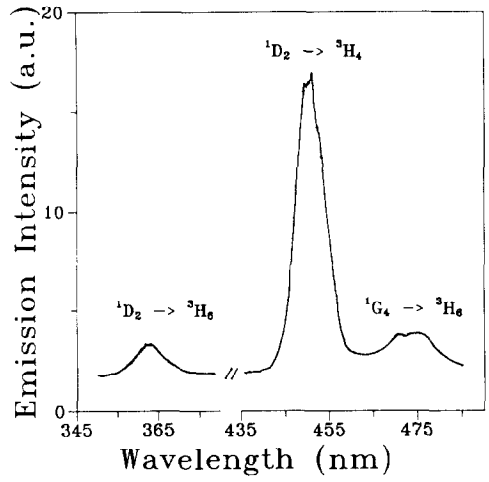

Fig. 3. Room temperature upconversion emission spectrum of the glass doped with $0.423 \times 10^{20}\,cm^{-3}\,Tm^{3+}$ ions.

Fig. 6 shows that the upconversion emission intensity depends quadratically on the excitation intensity for both 451 and 478 nm emissions. This result indicates that the $^1D_2$ and the $^1G_4$ levels are populated through a two photon process.

Emission spectra of the $^1D_2$ and $^1G_4$ levels were also obtained by exciting the desired level directly. When the $^1D_2$ level was excited with a 363 nm light no emission from the $^1G_4$ and the $^3F_4$ levels were observed. This means that these levels are not populated from the $^1D_2$ level directly and therefore the nonradiative transition rate of this level is small. The same result was predicted from the calculation of the radiative transition rates using the JO theory (Table 2). Emission from the $^3F_4$ level was however observed when the $^1G_4$ level was excited directly with 463 nm light.

Decay profiles of upconverted emissions from the $^1D_2$ and $^1G_4$ levels were also measured upon 657 nm pulsed excitation. In another words, the upconverted emissions from these levels were observed upon pulsed excitation. The Decay times

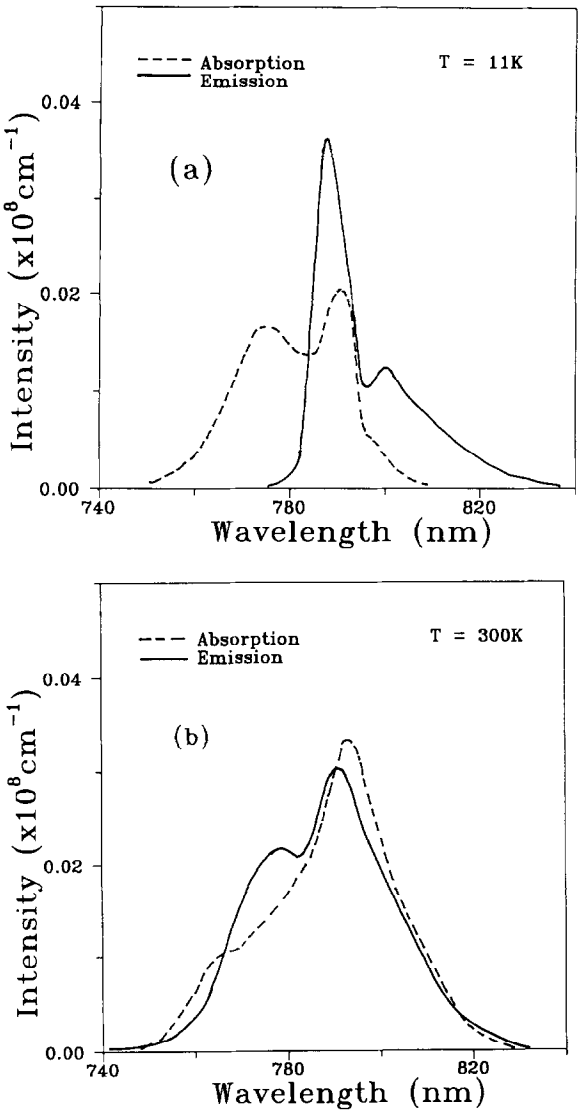

Fig. 4. Normalized absorption and emission spectra associated with the $^3F_4$ level in the glass doped with $0.423 \times 10^{20}\,cm^{-3}\,Tm^{3+}$ ions at (a) 11 K and (b) 300 K (the emission spectra were measured upon 657 nm excitation).

were found to be the same as those obtained by exciting each level directly (Table 3).

5. Interpretation of results

The origin of the emissions produced by upconversion of red light into shorter wavelengths can be

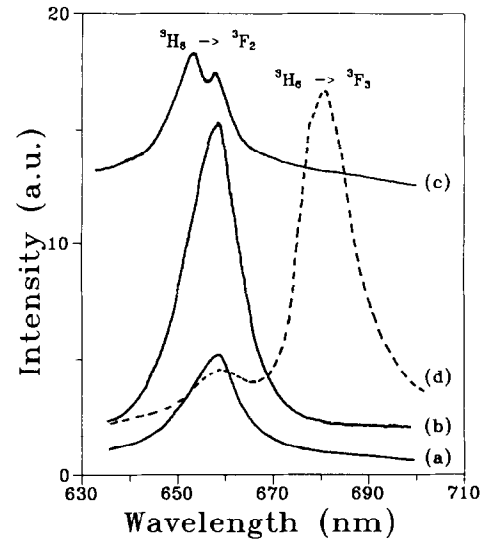

Fig. 5. Room temperature excitation spectra of the upconversion (a) 363 nm; (b) 451 nm; (c) 478 nm emissions, and (d): the downconversion emission from the $^3F_4$ level in the glass doped with $0.423 \times 10^{20}\,cm^{-3}\,Tm^{3+}$ ions in the 630 and 710 nm spectral region of the excitation light.

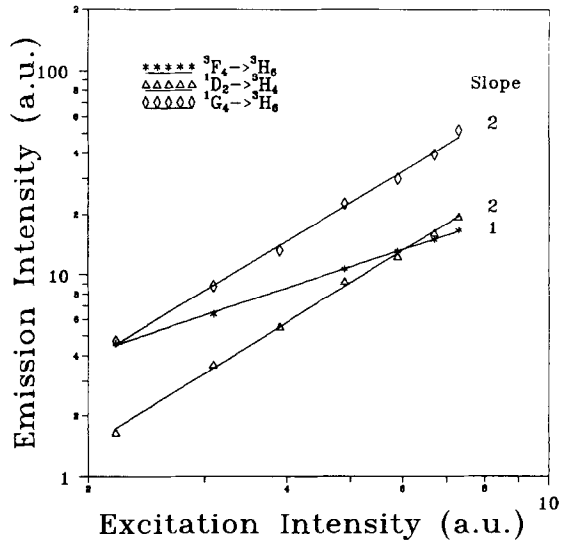

Fig. 6. Up- and down conversion emission intensities versus excitation intensity at 300 K (Δ, ◇ and * denote the emissions from the $^1D_2$, $^1G_4$ and $^3F_4$ levels, respectively).

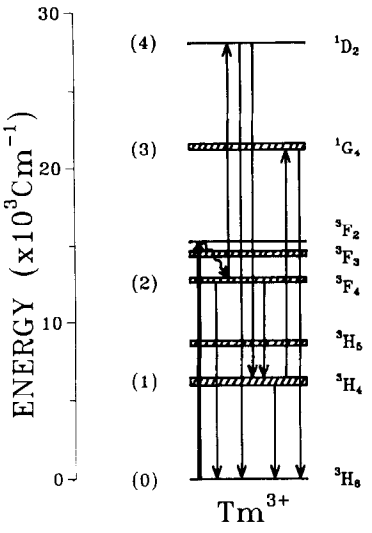

Fig. 7. The energy level diagram and the routes of the ESA processes.

understood by considering the energy level diagram for Tm^{3+} shown in Fig. 7. The mechanism is the multistep excitation by the ESA process [12]. An excited Tm^{3+} ion into the $^3F_2$ level with 657 nm light relaxes to the $^3F_4$ level via nonradiative transitions. The excited Tm^{3+} ion in the $^3F_4$ level is then raised to the $^1D_2$ level by the absorption of a second excitation photon. The ion in the $^3F_4$ level may also relax to the $^3H_4$ level via nonradiative transitions or via cross-relaxation processes due to the ion–ion interaction. If the second excitation photon is absorbed while the ion is in the $^3H_4$ level blue emission from the $^1G_4$ level centered at 478 nm is observed.

All of these processes may be described using a simple rate equation model. Fig. 7 also illustrates schematically the transitions involved where the notations to the right of each manifold denotes the energy level. When a Tm^{3+} ion is excited into the $^3F_2$ level with 657 nm radiation appropriate rate equations are:

$$\frac{dN_1}{dt} = W_{21}N_2 - (\sigma_{13}\phi + \tau_1^{-1})N_1,$$

$$\frac{dN_2}{dt} = \sigma_{02}\phi N_0 - (\sigma_{24}\phi + \tau_2^{-1})N_2, \qquad (1)$$

$$\frac{dN_3}{dt} = \sigma_{13}\phi N_1 - \tau_3^{-1}N_3,$$

$$\frac{dN_4}{dt} = \sigma_{24}\phi N_2 - \tau_4^{-1}N_4,$$

where τ_i is the radiative decay time of the ith excited level, σ_{ij} is the absorption cross-section for the transition from level i to level j and W_{ij} is the nonradiative transition rate from the ith level to the jth level.

The relationships between the populations of the excited levels can be obtained from Eq. (1) for continues beam excitation:

$$N_1 = \frac{W_{21}}{(\sigma_{13}\phi + \tau_1^{-1})}N_2,$$

$$N_2 = \frac{\sigma_{02}\phi N_0}{(\sigma_{24}\phi + \tau_2^{-1})}, \qquad (2)$$

$$N_3 = \tau_3\sigma_{13}\phi N_1,$$

$$N_4 = \tau_4\sigma_{24}\phi N_2.$$

As seen from these relationships the efficiency of an upconverted emission depends on the multistep excitation probability by ESA as well as the quantum efficiency of the emitting level. The probability of the multistep excitation is proportional to the lifetime of the intermediate excited states, for example upconversion efficiency of the emissions from the $^1D_2$ level depends on lifetime of the $^3F_4$ level.

The lifetime of an excited state is governed by the radiative and nonradiative decay processes and is given by

$$1/\tau = W_{RD} + W_P + W_E, \qquad (3)$$

where W_{RD} is the radiative decay rate, W_P is the multiphonon relaxation rate and W_E is the energy transfer rate due to the cross-relaxation process between ions. W_{RD} was caluclated using the JO theory. W_P is controlled by the phonon energy of the host and the energy difference to the next lower level. The phonon distribution is given by the Planck distribution [27] function $n(T)$ and usually is independent of the active ion concentration.

Fluorescence lifetime of the $^3F_4$ level strongly decreases when the thullium concentration increases since the lifetime of this level varies from 1.05 ms for 0.05 mol.% TmF_3 to 0.355 ms for 1.5 mol.% TmF_3 concentration. The strong shortening of the $^3F_4$ lifetime emphasizes very efficient Tm^{3+}–Tm^{3+} energy transfer processes. The dominant mechanism is the $^3F_4$, $^3H_6 \rightarrow {}^3H_4$, $^3F_4$ cross-relaxatio process [28]. This process competes with the fluorescence emissions of the $^3F_4$ level and is the dominant process in heavily doped compounds. We have confirmed this process in our glass by measuring the emission intensities from the $^3F_4$ and $^3H_4$ levels. We have found that the $^3H_4$ emission was very weak in the sample doped with 0.05 mol.% TmF_3 although it was stronger in the sample doped with 1.5 mol% TmF_3 while the intensity of $^3F_4$ emission was decreased. The cross-relaxation process was also confirmed by measuring the fluorescence quantum efficiency of the $^3F_4$ emission as function of Tm^{3+} concentration at room temperature. The fluorescence quantum efficiency of this level was determined using the equation: $\eta = \tau/\tau_R$ where τ and τ_R are measured fluorescence lifetime and calculated radiative lifetime of the level, respectively. Table 4, in which the values of η are presented, shows that the $^3F_4$ emission was quenched 65% by $^3F_4$, $^3H_6 \rightarrow {}^3H_4$, $^3H_4$ cross-relaxation process when the concentration of TmF_3 was 1.5 mol.%.

Rate of the energy transfer by means of cross-relaxation process due to ion–ion interaction depends on the separation between the ions R [22]. This dependence can be expressed in a multipolar expansion as follows:

$$W_E = c(6)/R(6) + C(8)/R(8) + C(10)/R(10) + \cdots, \tag{4}$$

where the first three terms correspond to dipole–dipole, dipole–quadruple an quadruple–quadruple interactions, respectively. If there is a dominant multipolar interaction then the transfer rate assumes the simpler form,

$$W_E = c(n)/R(n) = \varepsilon\tau_0^{-1}(R_0/R)^n. \tag{5}$$

In this expression, ε is the quantum efficiency of the donor luminescence in the absence of interaction between the Tm^{3+} ions. Normalized absorption and emission spectra of the $^3F_4$ level measured at 10 and 300 K and presented in Figs. 4(a) and (b) can be used to calculate spectral overlap integrals which are a measure of the ion–ion interaction rates at different temperatures. The critical interaction distance for a nonradiative electric dipole–dipole interaction mechanism is given by [29].

$$R_0^6 = \frac{3}{4\pi}\left(\frac{hc}{2\pi n}\right)^4 f_A \int \lambda^5 f_{em}(\lambda) f_{abs}(\lambda)\ \mathrm{d}\lambda, \tag{6}$$

where n is the refractive index of the sample, f_{em} and f_{abs} are the normalized emission and absorption spectra, respectively and f_A is the integrated absorption cross-section of the $^3F_4$ level and is

Table 4
Fluorescence quantum efficiencies of the $^1D_2$, $^1G_4$ and $^3F_4$ excited levels of Tm^{3+} versus Tm^{3+} concentration and of the $^3F_4$, $^3H_6 \rightarrow {}^3H_4$, $^3H_4$ the cross-relaxation energy transfer (C_{T_m} and η denotes Tm^{3+} concentration and quantum efficiency, respectively)

C_{T_m} [10^{20} cm^{-3}]	Fluorescence quantum efficiency [%] $\eta = \tau_F/\tau_R$			η[%] of the ($^3F_4$, $^3H_6 \rightarrow {}^3H_4$, $^3H_4$) cross-relaxation energy transfer $\eta = 1 - \tau_F/\tau_R$
	$^1D_2$ level	$^1G_4$ level	$^3F_4$ level	
0.106	41	40.0	56	44
0.202	40	41.0	51	49
0.423	41	36.5	39	61
0.635	38	36.0	42	58
1.267	40	36.0	29	71
2.101	39	35.0	23	77
3.133	36	33.5	20	80

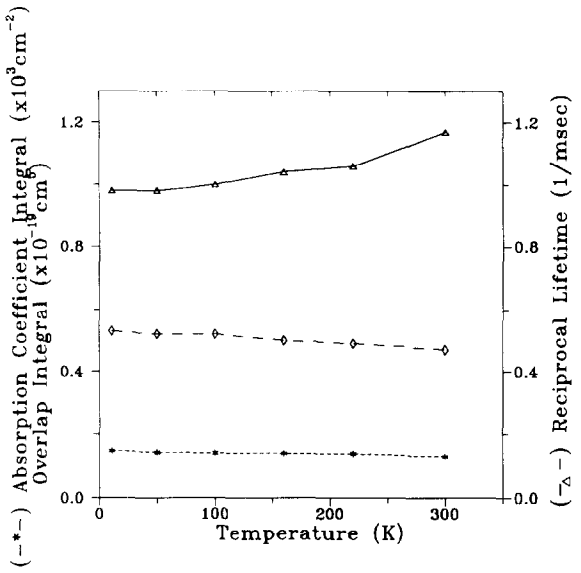

Fig. 8. The reciprocal lifetime (Δ), absorption coefficient integral (*) and the overlap integral (◇) for the $^3F_4$ level of Tm^{3+} ion in the glass doped with 0.423×10^{20} cm^{-3} Tm^{3+} ions as a function of the temperature.

$f_A = (mcn/2\pi^2 e^2 C_A)\int \sigma_A(\omega)d\omega$; where σ_A is the ground state absorption cross-section of ion A.

The reciprocal lifetime absorption coefficient integral and the overlap integral for the $^3F_4$ level were determined as function of temperature. The results are presented in Fig. 8. These results together with Eq. (5) were used to determine the Tm–Tm critical interaction distance. It is found to be almost independent of temperature in the 11 to 300 K range. These values and the microscopic interaction parameters in the dipole–dipole case are listed in Table 5.

According to the rate equation model under continues excitation the upconverted emission intensity depends on the excited state absorption cross-section (σ_{ESA}) corresponding to the $^3F_4 \rightarrow {}^1D_2$ transition for the emissions from the $^1D_2$ level and $^3H_4 \rightarrow {}^1G_4$ transition for the emissions from the $^1G_4$ level, fluorescence lifetime of the emitting level, excitation density and the population of the intermediate level. The excited state absorption intensity can be calculated using the following formula:

$$\frac{\int \sigma_{ESA}\, d\lambda}{\bar{\lambda}} = \frac{8\pi^2 e^2 (n+2)^2}{3ch(2J+1)9n} S_{ed}, \tag{7}$$

with

$$S_{ed} = \sum_{t=2,4,6} \Omega_t |\langle \alpha j \| U^{(t)} \| \beta j' \rangle|^2,$$

where $\bar{\lambda}$ is the average wavelength of the transition, $2J + 1 = 9$ is the degeneracy of the initial level such as $^3F_4$ and $^3H_4$ levels since they act as the initial levels for the second photon absorption resulting in the upconverted emissions from the $^1D_2$ and $^1G_4$ levels, respectively. S_{ed} is the electric dipole strength of the transition, Ω_2, Ω_4, and Ω_6 are the JO parameters and $U(t)$ are the double reduced matrix elements connecting the levels. Using the JO parameters calculated by us the excited state absorption intensity of the $^3F_4 \rightarrow {}^1D_2$ and $^3H_4 \rightarrow {}^1G_4$

Table 5
Temperature dependence of absorption cross section integral, overlap integral, lifetime, critical distance and the microscopic interaction parameter for the $^3F_4$ level of Tm^{3+} in the glass doped with 0.423×10^{20} cm^{-3} Tm^{3+} ions

$T[K]$	$\int \frac{1}{\lambda^2}\alpha_A(\lambda)\,d\lambda$ [$\times 10^2$ cm^{-2}]	$\int \lambda^6 g_A(\lambda) g_E(\lambda)\,d\lambda$ [$\times 10^{-20}$ cm^5]	R_0^6 [$\times 10^{-42}$ cm^6]	$\frac{1}{\tau}$[ms^{-1}]	R_0[Å]	C^6[$\times 10^{-42}$ s^{-1}]
11	1.49	5.3	44.77	1.167	18.84	52.25
50	1.43	5.2	42.15	1.060	18.65	44.68
100	1.41	5.2	41.38	1.037	18.59	42.62
160	1.40	5.0	39.66	1.030	18.47	40.85
220	1.39	4.9	38.68	1.000	18.39	38.68
300	1.25	4.7	33.30	0.833	17.93	27.74

transitions for the 657 nm excitation light have been calculated at 300 K. The results are listed in Table 6. Relatively low emission intensity of $^1G_4$ upconversion emission by ESA process can then be explained by the lower excited state absorption intensity of the $^3H_4$ level.

Fig. 9(a) presents the temperature variation of the 451 nm emission intensity and the decay time measured upon direct excitation. They both found to be independent of temperature. Temperature dependence of the 451 nm upconverted emission intensity upon red excitation is given in Fig. 9(b). The temperature dependence of the $^3F_4$ emission

Table 6
Excited absorption cross sections of $^3F_4 \rightarrow {}^1D_2$ and $^3H_4 \rightarrow {}^1G_4$ transitions in the Tm^{3+} doped fluorophosphate glass for 657 nm excitation wavelength at 300 K (σ_{ESA} denotes the excited state absorption cross-section in the table).

Transition	Matrix elements			$\int \sigma_{ESA} d\lambda$ $[10^{-6}]$
	$U(2)$	$U(4)$	$U(6)$	
$^3F_4 \rightarrow {}^1D_2$	0.1248	0.0096	0.2280	2.48
$^3H_4 \rightarrow {}^1G_4$	0.0020	0.0182	0.0693	0.19

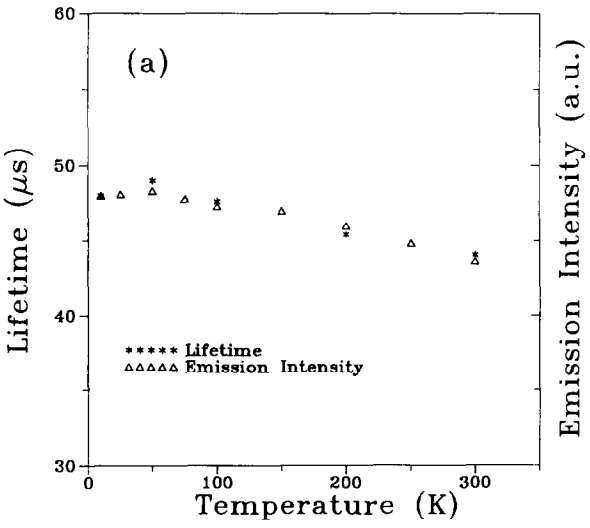

Fig. 9. Continued.

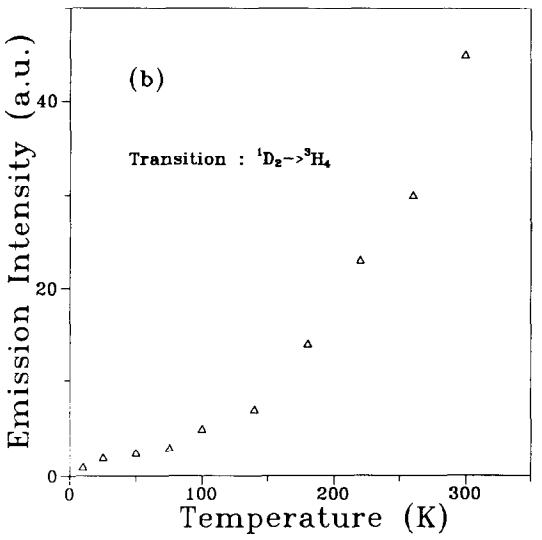

Fig. 9. (a) Integrated emission intensity and lifetime of $^1D_2$ level of Tm^{3+} ion in the glass doped with $0.423 \times 10^{20}\,cm^{-3}\,Tm^{3+}$ ions as function of temperature upon direct excitation (excitation source was either a Xe-lamp or a N_2 laser pumped molectron dye laser monitored at 363 nm). (b) Integrated emission intensity of $^1D_2$ level of Tm^{3+} ion in the glass doped with $0.423 \times 10^{20}\,cm^{-3}\,Tm^{3+}$ ions as function of temperature upon 657 nm excitation light.

intensity and the decay time obtained upon red excitation are depicted in Fig. 10. They both are independent of temperature below 100 K and they start decreasing above this temperature. Temperature dependence of the upconverted emission is due to the temperature dependence of the excited state absorption cross-section of the $^3F_4 \rightarrow {}^1D_2$ transition. This can easily be seen from the relationships between the excited state populations obtained from the rate equations for the steady state condition. Since the lifetime of the $^1D_2$ level, population of the intermediate level ($^3F_4$ level), and the excitation density are measured to be independent of temperature the temperature behavior of the $^1D_2$ upconverted emission is controlled by the temperature variation of the excited state absorption cross-section of the $^3F_4 \rightarrow {}^1D_2$ transition. The temperature dependence of this parameter is due to the change in the repopulation of the Stark levels of the levels involved in the upconversion process. Fig. 11

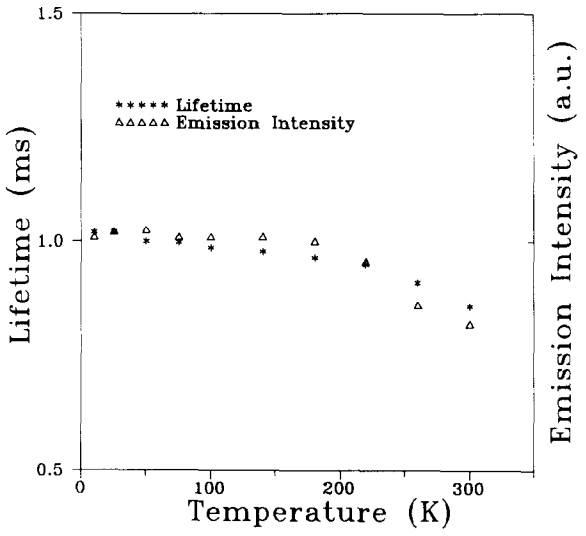

Fig. 10. Integrated intensity and lifetime of $^3F_4$ level of Tm^{3+} ions in the glass doped with $0.423 \times 10^{20}\,cm^{-3}\,Tm^{3+}$ ions ions upon 657 nm excitation.

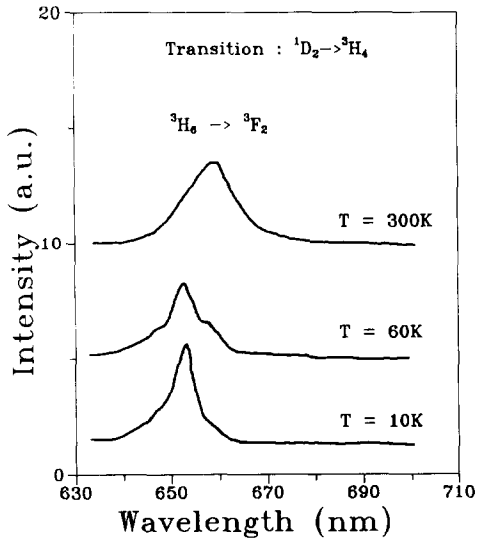

Fig. 11. Excited state excitation spectra of 451 nm emission corresponding to the $^1D_2 \rightarrow {}^3H_4$ transition in the glass doped with $0.423 \times 10^{20}\,cm^{-3}\,Tm^{3+}$ ions at different temperatures.

demonstrates the excited state excitation spectrum for the upconverted 451 nm emission at different temperatures. As it is seen from this figure, the absorption intensity of the second photon at 657 nm from the $^3F_4$ level increases with the temperature in the 10 to 300 K range.

6. Conclusion

The UV and blue upconversion fluorescences in Tm^{3+} doped fluorophosphate glass have been studied with the use of a tunable DCM dye laser for single wavelength pumping. Upconverted emission intensity of $^1D_2$ level was quenched due to the cross-relaxation process. Critical distance for this interaction was calculated using Dexters formula and was found to be independent of temperature with a value of 17.8 Å in the sample having a 0.2 mol.% TmF_3 concentration. Temperature dependence of the upconverted emission from the $^1D_2$ level was found to be controlled by the temperature variation of the excited state absorption cross-section corresponding to the $^3F_4 \rightarrow {}^1D_2$ transition. Higher upconversion emission intensity obtained at room temperature may make this glass interesting as an upconversion laser material.

Acknowledgements

We would kindly like to thank F. Auzel for helpful discussions. This work was partially supported by M.R.T. contract No 501444.

References

[1] M.F. Joubert, S. Guy, B. Jacquier, Phys. Rev. B 47 (1993), 11001.
[2] F. Auzel, Proc. IEEE 61 (1973) 758.
[3] F. Auzel, P. Pecile, D. Morin, J. Electrochem. Soc. 122 (1973) 101.
[4] O.L. Malta, P.A. Santa-Cruz, G.F. de Sá, F. Auzel, J. Solid State Chem. 68 (1987) 314.
[5] M. Pollnau, E. Heumann, G. Huber, Appl. Phys. A 54 (1992) 404.
[6] J.P. Jouart, C. Bissieux, G. Mary, J. Phys. C 20 (1987) 2019.
[7] J.C. Wright, Topics in Applied Physics, Vol. 15, ed. F.K. Fong (Springer, Berlin, 1976) p. 280.
[8] A.G. Makhanek, G.A. Skripko, Phys. Stat. Sol.(a) 53 (1979) 243.
[9] D.N. Rao, J. Prasad, P.N. Prasad, Phys. Rev. 28 (1983) 20.
[10] E.W.J.L. Oomen, J. Lumin 50 (1992) 317.

[11] J.Y. Allain, M. Monerie, H. Poignant, Electron. Lett. 26 (1990) 166.
[12] K. Hirao, K. Tamai, S. Tanabe, N. Soga, J. Non-Cryst. Solids 160 (1993) 261.
[13] F. Auzel, Rivista Della Staz. Sper. Vetro 5 (1990).
[14] S. Tanabe, S. Yoshii, K. Hirao, N. Soga, Phys. Rev. B 45 (1992) 4620.
[15] A. Kermaoui, C. Barthou, J.P. Denis, B. Blanzat, J. Lumin. 29 (1984).
[16] C. Guérey, J.L. Adam, J. Lucas, J. Lumin. 42 (1988) 181.
[17] Th. Weber, W. Lüthy, H.P. Weber, Appl. Phys. B 55 (1992) 144.
[18] B.R. Judd, Phys. Rev. 127 (1962) 750.
[19] G.S. Ofelt, J. Chem. Phys. 37 (1962) 511.
[20] F. Auzel, Ph. Degree Thesis (1968)
[21] D.L. Dexter, J. Chem. Phys. 21 (1953) 836.
[22] M. Inokuti, F. Hirayama, J. Chem. Phys. 43 (1963) 1978.
[23] G. Özen, J.P. Denis, XU Wu, A. Kermaoui, F. Pellé, B. Blanzat, J. Phys. Chem. Solids 54 (1993) 1533.
[24] A.A Kaminskii, Laser Crystals (Springer Verlag, 1981).
[25] R. Reisfeld, Y. Eckstein, J. Non-Cryst. Solids 15 (1974) 125.
[26] E.W. Duczynski, G. Huber, V.G. Ostroumov, I.A. Scherbakov, Appl. Phys. Lett. 48 (1986) 1562.
[27] C. Kittel, Introduction to Solid State Physics, 6th ed. (Wiley, New York, 1986) p. 101.
[28] A. Brenier, C. Pedrini, B. Moine, J.L. Adam, C. Pledel, Phys. Rev. B 41 (1993) 5364.
[29] B. Di Bartolo, Optical Interactions in Solids (Wiley, New York, 1968).